Indian J. Phys. **77B** (5), 503-512 (2003)

AN INTERNATIONAL JOURNAL
IJP B

Numerical modeling for the study of ozone transport in sea-breeze circulations at Sfax (Tunisia)

A Maalej[1]*, C Azri[2], K Medhioub[3] and R Rosset[4]

[1] Faculté des Sciences de Sfax (FSS), Département de Physique, 3018, Sfax, Tunisia
[2] Faculté des Sciences de Sfax (FSS), Département des Sciences de la Terre, 3018, Sfax, Tunisia
[3] Institute Préparatoire aux Etudes d'Ingénieurs de Sfax (IPEIS), Sfax, Tunisia
[4] Laboratoire d'Aérologie UMR CNRS/UPS 5560, 14 av. E. Belin, 31400, Toulouse, France

E-mail ahmedmaalej@yahoo.fr

Received 4 October 2002, accepted 24 June 2003

Abstract An ozone pollution episode typically at the mesoscale is studied for the summer period 14-15 July 1995 in the region of Sfax (Tunisia) which is submitted to strong sea-breeze circulations. At such regional scales, sea-breeze circulations are key dynamic features in the processing of natural and anthropogenic emissions in coastal, urban and industrial areas and inland, rural areas. The role of moving sea-breeze fronts on air pollution in the region of Sfax is investigated with the use of the mesoscale model Meso-NH-C (Mesoscale Non-Hydrostatic Chemistry model) in which the meteorological model Meso-NH is coupled on-line with a chemistry module. Various assumptions are presented for Meso-NH-C : *e.g.* compact of the chemical scheme to reduce the computational costs and the definition of procedures to fill in the lack of emission inventory data. Sensitivity studies about the impact of sea-breeze fronts on the transport and diffusion of ozone at coastal and inland areas of Sfax are presented. The Meso-NH appears to realistically simulate the sea-breeze circulations. Sea-breeze front penetration inland followed by its merging and interaction with strong continental convection caused an ozone dispersion in the period studied.

Keywords . Mesoscale modeling, sea-breeze circulations, pollution transport, ozone dispersion

PACS Nos. : 94.10.Fa, 92.60.Sz

1. Introduction

Comprehensive transport/chemistry models are quite effective tools for improving our knowledge of the mechanisms involved in air pollution episodes. Several studies using such models have been used to elucidate the effect of land-sea-breezes on air pollution transport in complex atmospheric-chemical environments [1-5].

In the present study, characteristics of the transport of ozone are investigated using a detailed coupled meteorology and chemistry mesoscale model Meso-NH-C [6]. This coupled model is applied to a typical situation of summer breezes in the region of Sfax [7], where few results have been published on air pollution in Sfax [8, 9]. These results concerning urban network measurements of gases and aerosols, can not be used in this regional study.

In this study, the first of its kind for Sfax, an industrial town at the Mediterranean shores of Tunisia (Figure 1), we had to make a gross estimation of emission fluxes of atmospheric pollutants. We have selected the typical summer situation on 14-15 July 1995. During this period, Meso-NH appears to realistically simulate the sea-breeze circulations using ECMWF (European Center for Medium range Weather Forecast) [10] data for the dynamic initialization.

2. The 14-15 July 1995 episode

2.1. Sea breeze development :

As regards the meteorological conditions in summer, the region of Sfax is usually sunny with a very dry land and a regular soil

* Corresponding Author

water deficiency from June. These climatological features result in the frequent development of sea-breezes in this Mediterranean region, almost every day in July and August. From the data collected at the Institut National de Météorologie (I.N.M), we have selected a set of July days in which sea-breeze circulations appear quite strong.

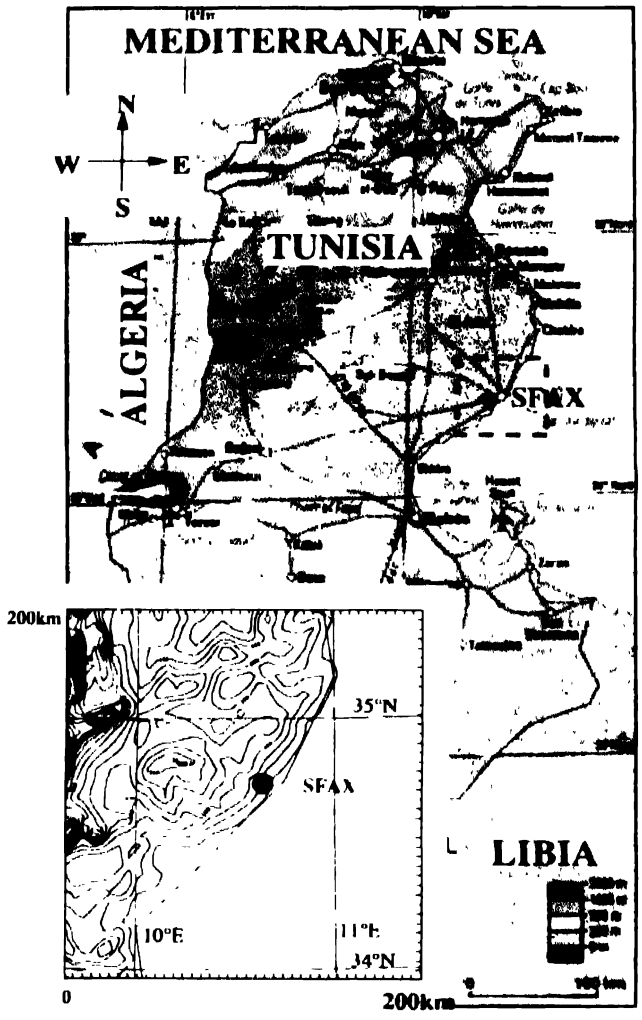

Figure 1. Location map of Sfax region in Tunisia : simulation domain (200km by 200km)

We have selected the case of July 14, 1995 characterized by a strong temperature gradient between land and sea (Figure 2a), at the origin of sea breezes.

In addition, the wind rose at Sfax meteorological station (Figure 2c) on that day, is also typical of sea-breezes episodes. With a clear anticorrelation between temperature and relative humidity in the presence of clear sky for this summer day (Figure 2b), we have simulated the dynamic circulation in the region of Sfax for cloudless sky.

2.2 *Regional ozone pollution :*

Only few results have been published upon detailed measurements of the pollution in Sfax [8,9]. In this study, only emission fluxes and initial concentrations of atmospheric pollutants estimates could be used. Ozone has been initialized with a single vertical profile : further explanation is given another section of this paper.

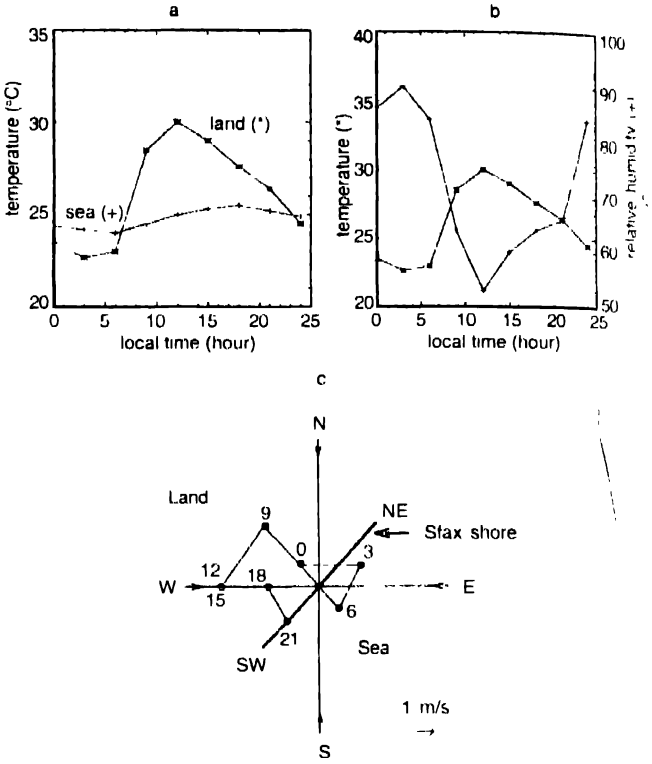

Figure 2. Diurnal variation of temperature over land and sea surface (a) (°C), of relative humidity (b) (%) and wind direction and strength (c), on July 14, 1995, at the shore station in the region of Sfax

3. Simulation of the 14-15 July 1995 pollution episode

3.1. *The Meso-NH meteorological model :*

The Meso-NH Atmospheric Simulation System [6] has jointly been developed by the Centre National de Recherches Météorologiques (CNRM/Meteo-France) and Laboratoire d'Aérologie (LA/CNRS). The Meso-NH model is a non hydrostatic numerical model covering a large range of atmospheric scales, from alpha to gamma scales [11]. This model relies on a comprehensive physical package, a set of initialization facilities, either idealized or interpolated from real meteorological analyses and/or forecasts. Some of the main characteristics of Meso-NH for our present purpose are as follows : an updated description of the land surface scheme ISBA (Interaction Soil Biosphere Atmosphere) is used, with recent improvements for evaporation from bare soils, the inclusion of gravitational soil drainage, a unified formulation of soil transfer coefficients for heat and moisture and a new version for surface drag coefficients [12].

The radiative scheme comprises two parts : solar visible radiation (ECMWF [10]), with the Madronich's scheme [13] used for ultraviolet (UV) and photochemistry.

Meso-NH is available in three (3D)-, two (2D)-, one(1D)- and zero (0D)- dimensional versions. The 3D and 0D (box) versions have been used here. In the following, 3D results will be displayed.

Nevertheless, some information about the particular use of the 0D version is necessary. This 0D model is not used in the usual Lagrangian mode for air mass transport. Instead, it is used in an Eulerian mode for two purposes. First, it gives a costless way of comparing the full EMEP (Evaluation Monitoring European Pollution) [14, 15] chemical scheme against the derived reduced scheme used in the study (see next paragraph). Secondly, apart from neglecting weak horizontal transport and with the assumption of instant vertical mixing below the inversion, this 0D (box) model allows for complex local chemical evolutions in the atmosphere under imposed emissions fluxes at the surface.

3.2 *The chemistry module :*

Chemistry modules coupled with three-dimensional (3D) meteorological models generally have to be reduced for different reasons. The first reason is obviously one of excessive computational costs. Second, due to severe limitations in experimental data bases, it is not possible to initialize most of the chemical species and to introduce detailed actual emission rates. This is why the full EMEP (LACTOZ) [14, 15] and LLOYD [16, 17] schemes (87 species and 166 reactions) have been reduced to 13 prognostic species and 19 reactions (Table 1). The criteria for this reduction are essentially based on the spectrum of hydrocarbon (VOCs) time scales in mesoscale pollution events [18]. According to Walcek and Yuan [19], one has introduced a hybrid class of VOCs (NMHC for Non-Methane HydroCarbons), assumed to be representative of polluted areas.

This reduction procedure has been developed under the constraint of optimal simulation of the ozone concentrations, since ozone is the species of particular interest here.

A more detailed account of the reduced chemical scheme is given in Table 1. A number of tests (not reported here for brevity) have been performed using this reduction procedure. These tests have been made using the Meso-NH 0D (box) version, both with the full EMEP and the reduced scheme. In these tests, it has clearly appeared that due to our reduction assumptions, the chemical scheme cannot apply in the immediate vicinity of emissions sources, but only at a distance [4]. In the present study, this reduced chemical scheme can be applied because the focus is on regional ozone distribution.

Table 1. The reduced chemical scheme with associated kinetic constants in s^{-1}, cm^3 molecule$^{-1}s^{-1}$, and cm^6 molecule^{-2} s^{-1}, respectively for first, second and third order reactions

Reaction			Kinetic constant
1	$NO + O_3$	$\rightarrow NO_2 + O_2$	$k_1 = 1.82 \times 10^{-14}$
2	$CO + OH$	$\rightarrow HO_2$	$k_2 = 2.41 \times 10^{-13}$
3	$HO_2 + NO$	$\rightarrow OH + NO_2$	$k_3 = 8.56 \times 10^{-12}$
4	$NO_2 + OH$	$\rightarrow HNO_3$	$k_4 = 1.14 \times 10^{-11}$
5	$CH_4 + OH$	$\rightarrow RO_2$	$k_5 = 6.45 \times 10^{-15}$
6	NMHC + OH	$\rightarrow RO_2$	$k_6 = 4.13 \times 10^{-11}$
7	$RO_2 + NO$	$\rightarrow NO_2 + HO_2 + RCHO$	$k_7 = 9 \times 10^{-12}$
8	$OH + HO_2$	$\rightarrow$ loss	$k_8 = 1.11 \times 10^{-10}$
9	$HO_2 + HO_2$	$\rightarrow$ loss	$k_9 = 5.45 \times 10^{-12}$
10	$RCHO + OH$	$\rightarrow RCO_3 + H_2O$	$k_{10} = 1.76 \times 10^{-11}$
11	$RCO_3 + NO_2$	$\rightarrow$ PAN	$k_{11} = 6.81 \times 10^{-12}$
12	PAN	$\rightarrow RCO_3 + NO_2$	$k_{12} = 7.86 \times 10^{-4}$
13	NO_2	$\rightarrow O_3 + NO$	$J_{NO2} = 1.1 \times 10^{-2}$
14	O_3	$\rightarrow 2OH$	$J_{O3} = 5.1 \times 10^{-6}$
15	RCHO	$\rightarrow CO + 2HO_2$	$J_{CHOH} = 2.4 \times 10^{-5}$
16	RCHO	$\rightarrow CO$	$J_{COH2} = 3.6 \times 10^{-5}$
17	RCHO	$\rightarrow RO_2 + HO_2 + CO$	$J_{CH3CHO} = 5.1 \times 10^{-6}$
18	RCHO	$\rightarrow RO_2 + HO_2 + CO$	$J_{P1CHO} = 4.2 \times 10^{-5}$
19	RCHO	$\rightarrow RO_2 + HO_2 + CO$	$J_{P2CHO} = 4.2 \times 10^{-5}$

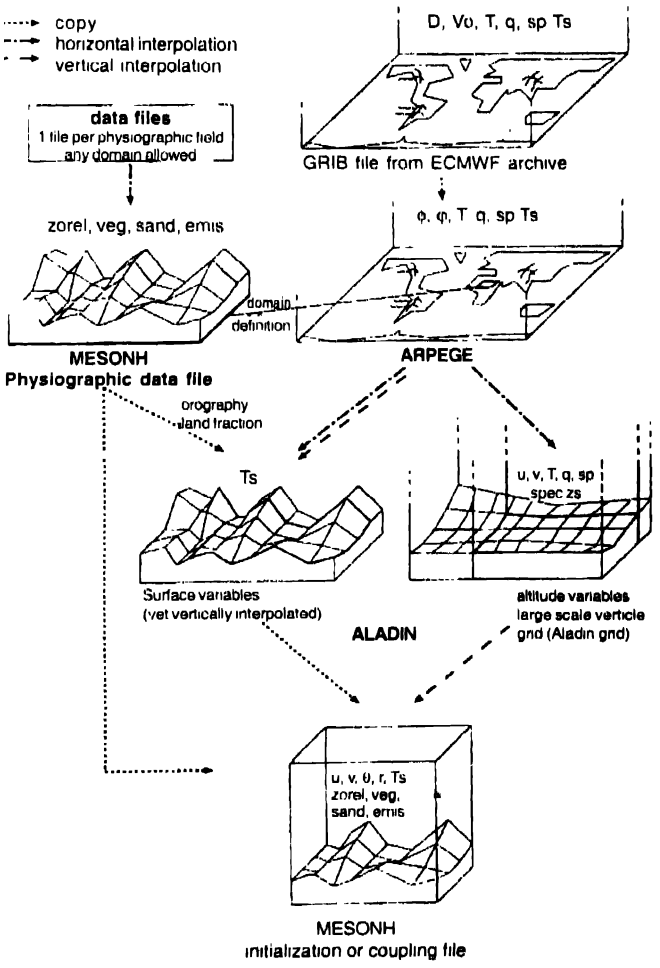

sp surface pressure, spec zs spectral orography (large-scale orography), D divergence, Vo vorticity, Ts (temperature of surface) stands for all other surface variables temperatures, water and snow contents, zorel, vew, sand, emis stand respectively for orographic, vegetation, soil and radiation PGDfiles.

Figure 3. Schematic view of the interactions between the different files during the initialization sequence of a real case simulation

3.3. Simulation characteristics :

The simulation of realistic meteorological situations is an important scope of Meso-NH. The preparation of initial fields by interpolation of larger-scale meteorological analyses of forecasts, in a format ready to start a Meso-NH experiment, is therefore an important task. The Meso-NH initial file is obtained by the combination of physiographic and Aladin meteorological data files (Figure 3).

The Aldin file containing meteorological fields are extracted from ECMWF or Meteo-France operational archives. We take advantage of the fact that the Aladin model of Meteo-France [20] works with the same conformal projections as Meso-NH to minimize the number of horizontal interpolations aiming to preserve the integrity of the meteorological information. The dynamical fields are first initialized and then subsequently forced as boundary conditions in Meso-NH using the French operational ARPEGE model analyses [21].

A physiographic data file is needed in order to specify the geographical domain for the Meso-NH simulation and to initialize general data about the surface (land-sea mask, orography, vegetation, ground composition, albedo,....). The physiographic data are grouped into four categories (*i.e.*, the geographic fields, the soil and vegetation characteristics, and the fields related to the radiation), as shown in Table 2. In the region of Sfax, the surface data necessary to construct this physiographic file is not available. We have used default fields.

Table 2. List of the entry surface fields

Geography	Land-sea-lake mask	0 sea , 1 land , 2 lake or inland-water
	Z_S	Topography
	$Z_{0\,rel}$	Roughness length of the relief (optional , can be recalculated from orography)
Soil	clay	Clay fraction of the ground
	sand	Sand fraction of the ground
Vegetation	veg	Fraction of vegetation
	d_2	Depth of the soil column
	LAI	Leaf area index
	C_v	Heat capacity of the vegetation
	$Z_{0\,veg}$	Roughness length of the vegetation
	$Z_{0h\,veg}$	Thermal Roughness length of the vegetation
	R_{smin}	Minimum stomatal resistance
Radiation	α_{vis}	Albedo for the solar radiation
	α_{ir}	Albedo for the infrared radiation
	ε	Emissivity

Of course, these fields have relatively coarse resolution, of the order of one degree, but they are global, and thus assure the Meso-NH users that reasonable surface characteristics will be considered in their simulation. These default surface fields in the Table 2, are created as follows :

(i) The land-sea-lake mask field has a resolution of 1 minute. It is taken from the Micro World Data Bank II

(ii) The topography field has a resolution of 5 minutes. It is taken from the TerrainBase database [22].

(iii) The soil characteristics, *i.e.*, the clay and soil fields, are directly read from the Webb *et al* classification [23], with an horizontal resolution of 1 degree

(iv) Many other surface fields are derived from the type of vegetation, which is classified according to Wilson *et al* [24] and represented on 1-degree grid.

(v) The albedos are obtained from values deduced from the color of the soil and the type of vegetation following correspondence tables given in Wilson *et al* [24].

These surface fields are used in the ISBA model for the evaluation of the surface fluxes of momentum, sensible heat, and moisture, as well as the evolution of prognostic variables (the surface temperature, the mean temperature, the soil moisture, ...).

The geographical domain selected is large enough (200 km by 200km horizontally and 4000m vertically) (Figure 1) The horizontal grid resolution is 5km against 62m in vertical resolution near the surface regularly increasing to 600m at the top of the model. We have 32 vertical levels ranging from the lowest level (0m) and the top level (4000m).

We will follow the dynamics and chemistry evolutions for a period of two successive days (14-15 July 1995). The beginning of the simulations is the 14 July 1995 just before sunrise (0600 LST).

3.4. Chemical initialization :

3.4.1. Vertical profiles of chemical species

The prognostic chemical species of the coupled dynamic physico-chemical model (Meso-NH-C), are initialized by vertical profiles.

In this study, severe limitations are due to the lack of experimental data. In the simulations, ozone is initialized with a vertical profile. High concentrations of ozone in the free troposphere, progressively decrease in the boundary layer due to the activation of oxidation reactions and dry deposition near the surface.

A vertical profile for ozone has been defined for 0600 LST (just before sunrise), at the beginning of the simulations (Figure 4). In this profile, ozone concentrations have a constant value of 54 ppb over 2000m. Below this height, there is a linear decrease in ozone concentrations down to 35 ppb near the surface. For

other prognostic species, a constant vertical profile is imposed (Table 3).

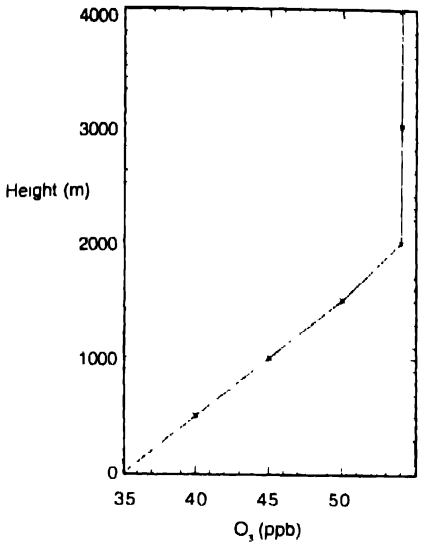

Figure 4. Estimated vertical profile for ozone at 0600 LST in the lower troposphere of the region of Sfax

Ozone and the other 12 prognostic species (Table 3) are coupled with the meteorological model Meso-NH. At each time step of Meso-NH at each physical grid point, a set of 'stiff' differential equations (the lifetime of the different chemical species may vary by upto ten orders of magnitudes) describing the chemical evolution of the prognostic species is solved. Also at each step and each time step, the reaction and photolysis rates are calculated as a function of the meteorological variables temperature, pressure, humidity,....

Table 3. Initialisation of chemical species concentrations

Chemical species	initial value (ppb)
NO	0 05
NO_2	0 1
HNO_3	0.1
OH	0
HO_2	0
CO	120
CH_4	1700
NMHC	10
RO_2	0
RCHO	2
RCO_3	0
PAN	2

The reaction scheme that is presently implemented, contains 13 chemical species and 19 photo-chemical reactions (Table 1)

The boundary conditions, advection and turbulent transport of chemical species are treated in the same way as for the Meso-NH water variables [25].

3.4.2. Chemical emissions

There is presently no detailed emission inventory available for the Sfax region, at required space and time resolutions. Our purpose here is to define an order-of-magnitude estimate chemical emission sources in the simulation domain.

On the continent, zonation of the Sfax region (Figure 5) indicates the different emission zones according to the horizontal resolution of the model. We imposed the surface emission rates for every emitted species in each surface grid cell ($5 \times 5 km^2$) of the simulation domain. The values of surface emissions fluxes for nitrogen oxides (NOx) and NMHC for the different ecosystems are presented in Table 3. The emission rates from the different ecosystems being generally greater during the day than at night, we have imposed an emission flux of NOx and NMHC five times larger during the day than at night (Table 4). The maritime emissions of NOx and NMHC are neglected [26, 27]

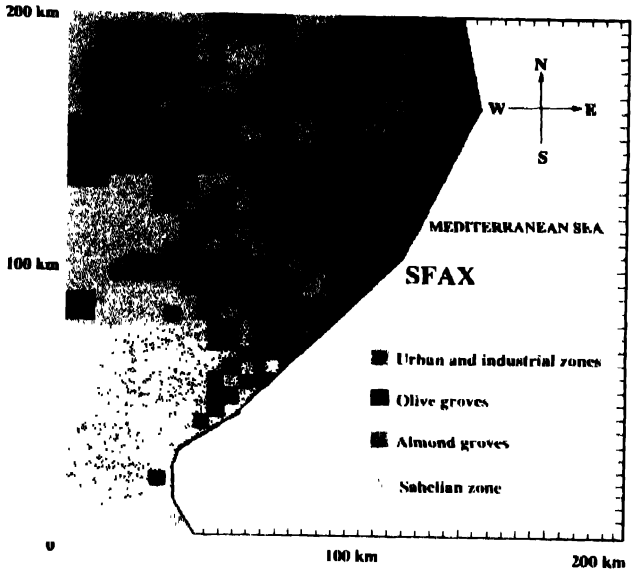

Figure 5. Urban zone and vegetation cover in the region of Sfax

Table 4. Estimated NOx and NMHC emissions for the different ecosystems from the region of Sfax

	Surface flux (molecule $cm^{-2}s^{-1}$)*		
	NO	NO_2	NMHC
Urban and industrial zones	10^{13}	10^{12}	5×10^{12}
Olive groves	10^{11}	10^{10}	10^{11}
Almond groves	10^{11}	10^{10}	10^{12}
Sahelian zone	10^{10}	10^{9}	10^{10}

* nocturnal value divided by 5.

4. The 14-15 July 1995 episode modeling results

4.1 Simulated sea-breezes :

On July 14, 1995, a typical sea-breeze development is observed (Figure 6). Inland penetration of sea-breeze front

develops during the day, reaching 80 km at 1800 LST. At midnight, reversal of the flow is observed, with a weak land-breeze circulation.

To illustrate the sea-breeze development and its impact on the transport and diffusion of coastal pollutants, a vertical cross section is displayed along the AB transect of the three

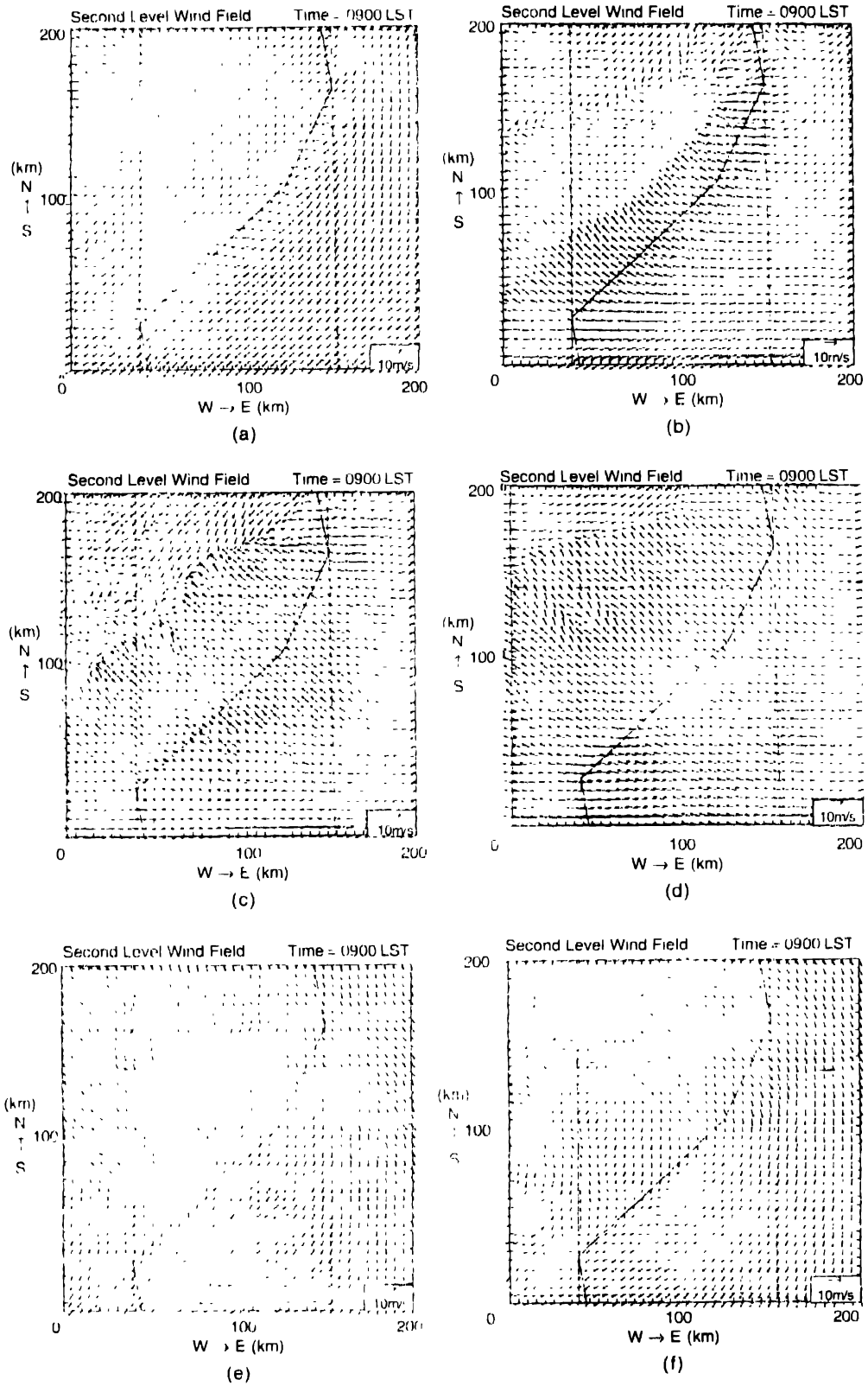

Figure 6. Simulated sea breeze at second model level (62m) : (a) at 0900 LST ; (b) at 1200 LST ; (c) at 1500 LST , (d) at 1800 LST , (e) at 0000 LST ; (f) at 0600 LST (July 14 and 15, 1995). The arrow on the lower right corner is for 10 ms^{-1}

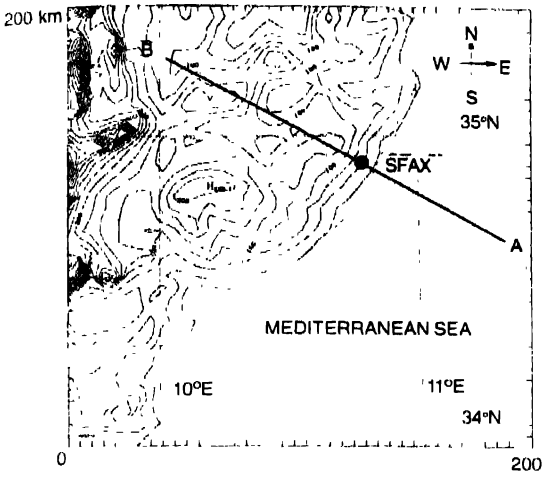

Figure 7 Horizontal section of the Meso-NH domain over the region of Sfax (Tunisia) (topographic heights every 25m); AB is the vertical cross section in the following

dimensional field (Figure 7). In this transect, total wind velocities and turbulent kinetic energies are superimposed (Figure 8).

At 07007 LST, very low wind speeds are observed in the very stable boundary layer. At noon, there is deepening of the mixed layer with strong sea-breeze circulation together with separated strong convection inland.

At 1600 LST, the inland penetration of the sea-breeze front reaches about 70 km, quite close to the convection zone inland. The mixed layer reaches a height of about 3000 m with an elevated area of turbulent kinetic energy probably due to wind shear.

Then, at 1900 and 2100 LST, with reduced surface heating, turbulent kinetic energy is decreased. Nevertheless, we still observe further penetration towards inland of the sea-breeze

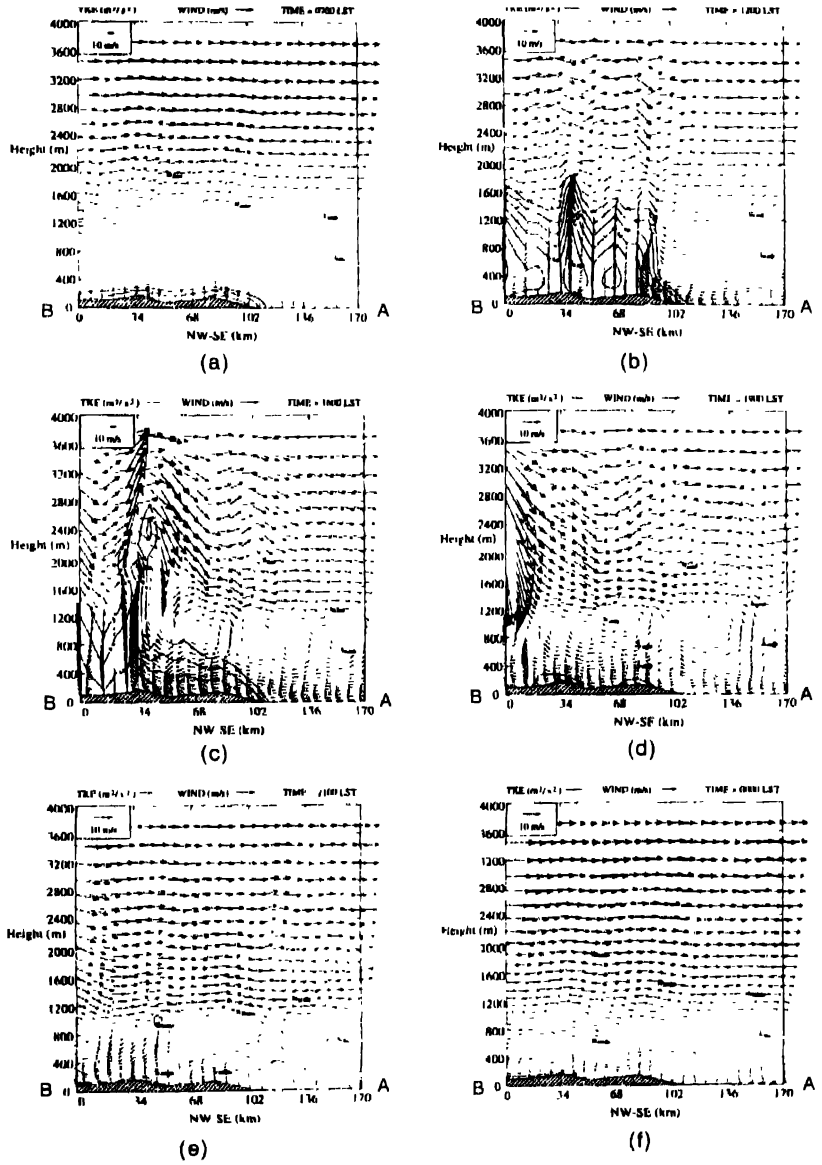

Figure 8. Vertical cross section along AB transect for total wind velocity and turbulent kinetic energy (July 14, 1995) : (a) at 0700 LST ; (b) at 1200 LST, (c) at 1600 LST , (d) at 1900 LST. (e) at 2100 LST; (f) at 0000 LST.

front. At midnight, a light land-breeze circulation is observed, corresponding to reversal of the flow near the surface.

4.2. Ozone evolution :

Ozone and the distribution of its precursors in the low troposphere, mainly results from the strength of surface emissions of nitrogen oxide (NOx) and non-methane hydrocarbons (NMHC), as well as the meteorological conditions leading to accumulation of these trace gases in the urban and rural areas of Sfax. Sea-breeze circulations are the major meteorological phenomena affecting the pollutant distribution at this period of the year.

In this work, we only display the ozone evolution in 3D perspective (Figures 9, 10, 11). During the simulation, we have illustrated the effect of sea-breeze penetration inland. Interpretation of this 3D evolution becomes easier for considering the impacts of sea-breeze and continental convection (reference to horizontal cross sections at second model level (62m) (Figures 12, 13)). The model has been run during two diurnal cycles (July 14 and 15, 1995).

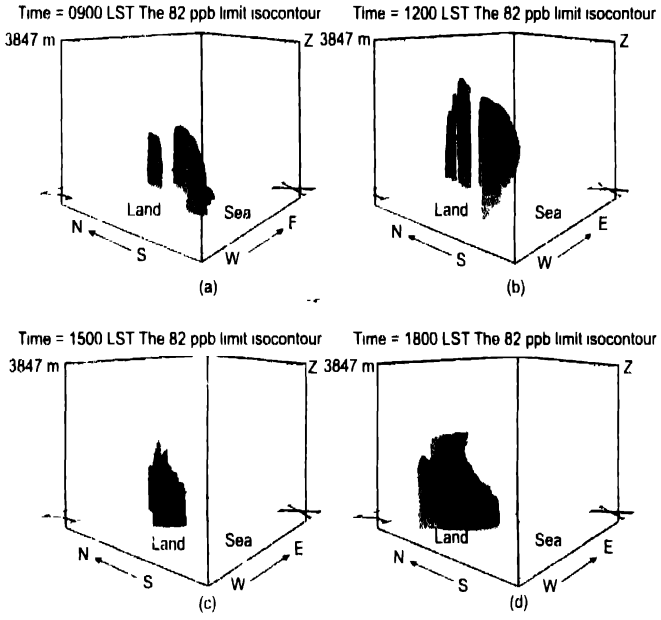

Figure 9. Simulated ozone (O_3) concentrations during 33 hours. The 'reading' of this figure becomes easier for considering the impacts of sea-breeze circulation and continental convection (reference to horizontal cross sections 12, 13) (a) 0900 LST; (b) 1200 LST, (c) 1500 LST, (d) 1800 LST, on July 14 1995 (represented in 3D perspective only, the concentrations greater than 82 ppb

Ozone is produced by NO_2 photolysis in the proposed chemical scheme (reaction (13), Table 1 [4, 14, 15]). It is destroyed by photodissociation (reaction (14), Table 1 [4, 14, 15]) and is partially titrated near the surface by reaction (1) in Table 1.

Only July 14, 1995 at 0900 LST (Figure 9a), after three hours of simulation ozone concentration exceeds 82 ppb over the urban and industrial areas of Sfax, which are strong emitters of NO_x (Figure 12a).

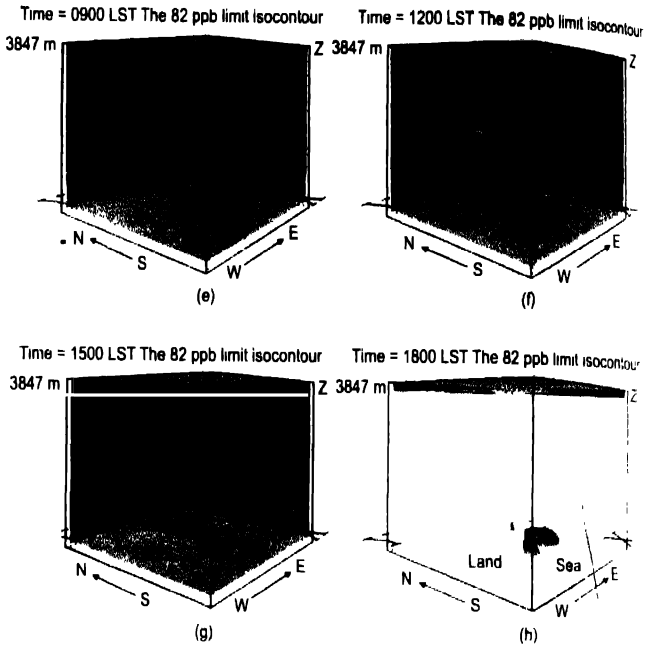

Figure 10. (e) 2100 LST, (f) 0000 LST, (g) 0300 LST, (h) 0600 LST, on July 14 and 15 1995 (Represented in 3D perspective only, the concentrations greater than 35 ppb for (e,f,g) and 51 ppb for (h) (continuation))

This ozone production is due to NO_2 photolysis activated from sunrise (at 0600 LST). The effect of land convection is significant with upward transport of ozone within the convective boundary layer.

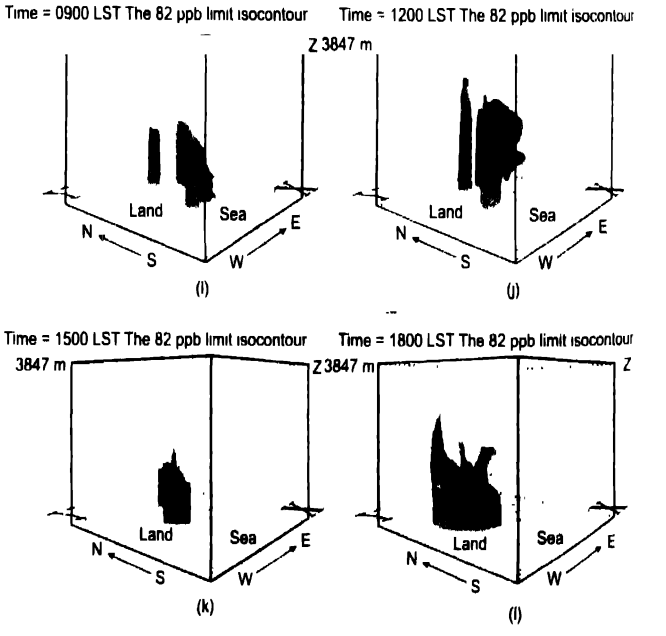

Figure 11. (i) 0900 LST, (j) 1200 LST, (k) 1500 LST, (l) 0600 LST on July 15 1995. (represented in 3D perspective only, the concentrations greater than 82 ppb (end)).

At 1200 LST (Figure 9b), the effect of combined convective development and inland penetration of the sea breeze on ozone distribution is quite significant. Ozone is displaced in the lower layers by the sea breeze with a maximum of concentration at the front level about 20 km from the coast. Over urban and industrial areas, the loss of ozone is due to the transport of this pollutant by sea breeze front followed with ozone reaction with NO strongly emitted in these areas (Figure 12b).

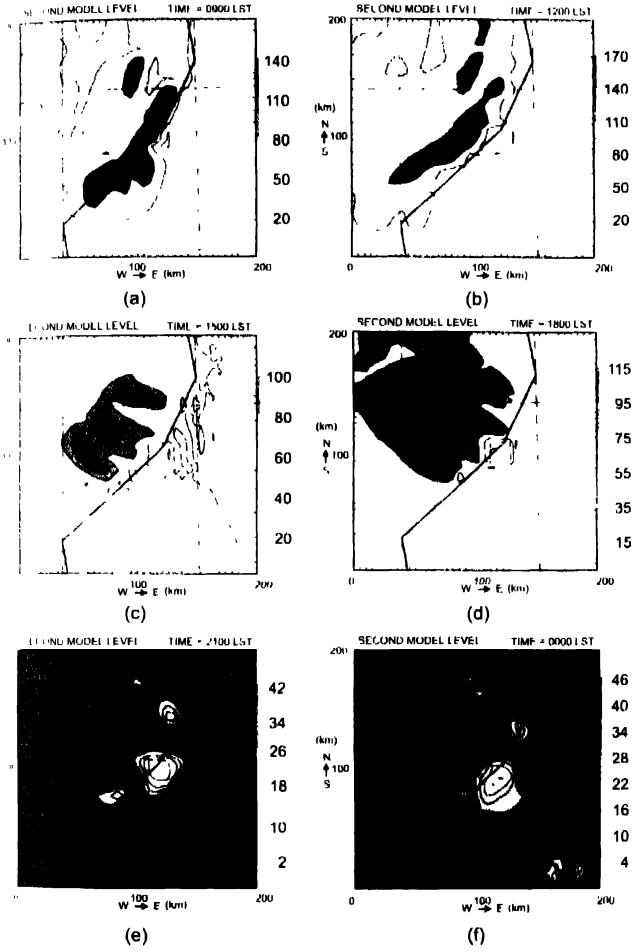

Figure 12. Horizontal cross section for simulated ozone (O_3) (ppb) along the second model level (62m), during 33 hours (a) 0900 LST, (b) 1200 LST, (c) 1500 LST, (d) 1800 LST; (e) 2100 LST; (f) 0000 LST, on July 14 1995. Contours, in intervals of 30 ppb for (a, b), of 20 ppb for (c, d), of 8 ppb for (e) and of 6 ppb for (f)

At 1500 LST (Figure 9c), ozone is displaced in land by the sea breeze front. In the lower layers (Figure 12c), ozone concentrations exceed 60 ppb at the sea-breeze front in rural areas, where three cells included a maximum of ozone concentrations over 80 ppb. These cells are located over the sahelian zone (Figure 5), where low NOx emission occurs. Over Sfax urban and industrial areas, ozone loss is quite remarkable, with ozone concentrations lower than 40 ppb as compared to ozone increase in rural areas (over 80 ppb). This loss is explained both, by the transport of ozone from the coast by the sea-breeze front and the strong NOx emissions in urban areas favoring trapping of ozone by its reaction with NO.

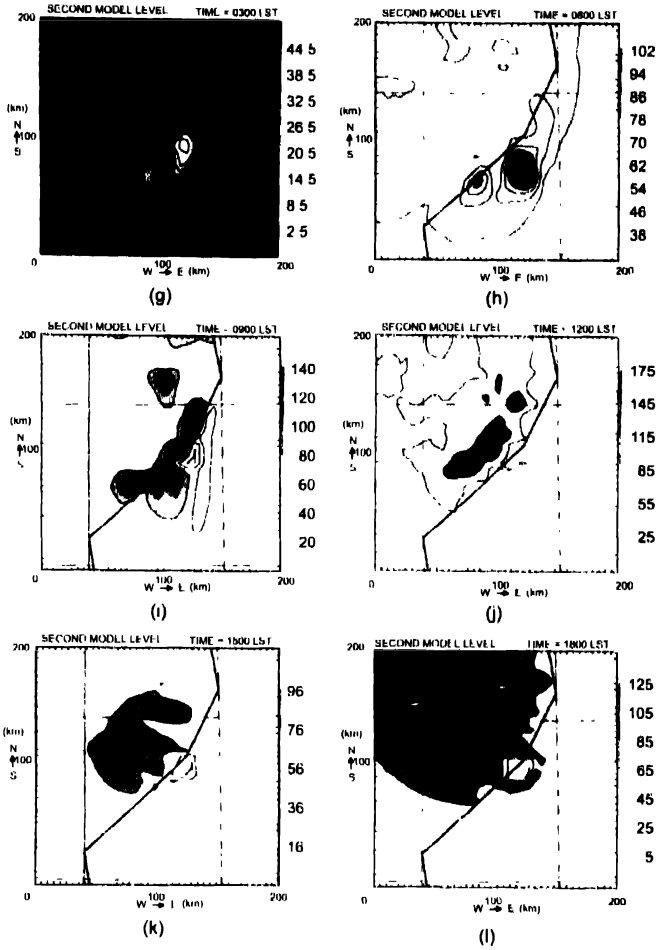

Figure 13. (g) 0300 LST, (h) 0600 LST, (i) 0900 LST, (j) 1200 LST, (k) 1500 LST; (l) 1800 LST, on July 15 1995. Contours, in intervals of 6 ppb for (g), of 8 ppb for (h), of 20 ppb for (i, k, l) and of 30 ppb for (j) (end)

At 1800 LST (Figure 9d), ozone transported by the sea-breeze front reaches strong convection zone as much as 80 km inland (Figure 8c). The impact of this continental convection appears by a strong upward flow of ozone at a level of interaction zone between this convection and sea-breeze front. In a lower layer (Figure 12d), three cells having a strong ozone concentration, are displaced in land by sea-breeze front. The central cell, the most displaced one, is located along the direction of sea-breeze inland penetration (Figure 6d).

At night of July 14, 1995, from 2100 LST to 0300 LST of July 15, 1995, in absence of solar radiation, there is no production of ozone by NO_2 photolysis. The reaction of ozone with NO determines a significant decrease of ozone near the urban and industrial areas characterized by strong NO emission rates. This loss of ozone appears in Figures 10 (e, f, g) by the convex surfaces observed over urban areas. Ozone concentrations are lower than 35 ppb under these surfaces. This nocturnal destruction of ozone

also appears in the horizontal cross sections at the second model level (62m) (Figures 12, e, f and 13g). In these low layers, the effect of the weak land-breeze is shown by the transport of ozone over the sea. In 3D perspective, Figures 10 (e, f, g) show the stability of nocturnal boundary layer with stratified ozone in altitude (*i e.* progressive increase of ozone concentration from the surface to the free troposphere). At sunrise (0600 LST) on July 15, 1995 (Figure 10h), there is a spectacular and rapid increase of ozone concentrations near urban and industrial areas, which are strong sources of NOx This increase of ozone is explained by activation, just after sunrise, of the chemical production of ozone by photodissociation of NO_2 In low layers, the effect of the weak land-breeze near the surface is still observed ; ozone generated over urban areas is displaced towards the sea by the land-breeze (Figure 13h).

On July 15, 1995 at 0900 LST, 1200 LST, 1500 LST and 1800 LST respectively (Figure 11 i, j, k, l), we observe an ozone evolution similar to the one on the day of July 14. Such a similarity is to be found in the analogy of atmospheric circulations on July 14 and 15, 1995, under the dominance of sea-breeze circulations and continental convection (Figures i, j, k, l). In addition, ozone formed on July 14, 1995 is completely displaced out of the simulation domain :

- in low layers, by inland penetration of the sea-breeze front.
- at altitude, by the synoptic winds after strong upward transport due to the interaction between the sea-breeze front and continental convection (Figure 8c).

On July 15, 1995, there is no ozone accumulation after the two previous diurnal cycles, with only addition of residual ozone at the end of July 14 day (only 35 ppb) and ozone subsequently formed on July 15.

5. Some conclusions and perspectives

An ozone pollution episode has been studied in the region of Sfax on 14 and 15 July of 1995. During this period, Meso-NH model appears to realistically simulate the sea-breeze circulations. Sea-breeze front penetration in land followed by its merging and interaction with continental convection has been analyzed.

Implementation of reactional chemistry in the dynamic circulations of 14 and 15 July, 1995 shows the effect of sea-breeze front penetration and continental convection on the formation, transport and distribution of ozone.

In this study, after two diurnal cycles (14 and 15 July), we have not observed an ozone accumulation over the region of Sfax :

- in the low layers, the sea-breeze has displaced inland the ozone generated at the coast.
- at altitude, the synoptic wind has displaced ozone, after strong upward transport due to interaction between the sea-breeze front and continental convection.

Several improvements could be expected by installing some urban and rural stations in the region of Sfax, extending and refining the chemical scheme and perhaps more important by better documenting the emission source inventory.

References

[1] T Kitada and E Kitagawa *Atmos Environ* **24A** 1545 (1990)

[2] R Romero and C Ramis *Ann Geophysicae* **14** 351 (1996)

[3] R Lu and R P Turco *Atmos. Environ* **30** 4155 (1996)

[4] P Tulet, A Maalej, V Crassier and R Rosset *Atmos Environ* 33 1651 (1999)

[5] A Lemonsu and V Masson *Boundary Layer Meteorology* **104** 463 (2002)

[6] J P Lafoie, J Stein, A Asencio, P Bougeault, V Ducrocq, J Duron C Fischer, P Hériel, P Mascart, V Masson, J P Pinty, J L Redelsperger, E Richard and J Vilà-Guerau de Arellano *Ann Geophysicae.* **16** 90 (1998)

[7] Atlas du Gouvernorat de Sfax (1994)

[8] C Azri, A Maalej and K Medhioub *Pollution Atmosphérique* **NO165** 121 (2000)

[9] C Azri, A Maalej, A Tili and K Medhioub *Technique Science Méthode* (T S M) No 1, 78 (2002)

[10] J J Morcrette *Technical Memo* 165 (Res Dep ECMWF Readin England) (1989)

[11] I Orlanski *Bull Am Meteorol Soc* **56** 527 (1975)

[12] B Jacquemin and J Noilhan *Boundary-Layer Met* **52** 93 (1990)

[13] S Madronich *J. Geophys Res* **92** 9740 (1987)

[14] D Simpson *Atmos Environ* **26 A** 1609 (1992)

[15] LACTOZ, Rapport EMEP MSC-W OZONE MODEL Wuppertal (1993)

[16] A C Lloyd, R Atkinson, F W Lurmann and B Nitta *Atmos Environ* **17** 1931 (1983)

[17] A Maalej *Ph D. Thesis* (Université Paul Sabatier, Toulouse III France) (1997)

[18] J H Seinfeld and S N Pandis *Atmospheric Chemistry and Physics* (New York John Wiley) (1998)

[19] H Walcek and H Yuan *Computation Mechanics Publications* (1996)

[20] W Sadiki, C Fischer and J F Geleyn *Mon Wea. Rev* **128** 3927 (2000)

[21] M Deque, C Dreveton, A Braun and D Cariolle *Climate Dyn* **10** 249 (1994)

[22] L W Row and D Hastings *National Geophysical Data Center and World Data Center A for Solid Earth Geophysics* (Boulder, Colorado USA)

[23] R S Webb, C E Rosenzweig and E R Levine *A global data set of soil particle size properties* (New York : NASA Goddard Institute of Space Studies) (1991)

[24] M F Wilson, A Henderson-Sellers, R E Dickinson and P J Kennedy *J Appl Meteor* **26** 341 (1987)

[25] *The Meso-NH Atmospheric Simulation System* : Météo-France CNRM (1995)

[26] M Kanakidou and P J Crutzen *Chemosphere* **26** 787 (1993)

[27] J Matthijsen *Ph D Thesis* (University of Utrecht, Netherlands) (1995)